The Ninth International Conference on Synchrotron Radiation Instrumentation
May 28 – June 2, 2006, DAEGU, EXCO, KOREA

DEVELOPMENT OF A PLANAR UNDULATOR

Alex Deyhim, Eric Johnson, Joe Kulesza, Aaron Lyndaker, Dave Waterman, Dave Eisert*, Michael A. Green*, Greg Rogers*, K. Ingvar Blomqvist**

Advanced Design Consulting USA, 126 Ridge Road, P.O. Box 187, Lansing, NY 14882, USA
** Synchrotron Radiation Center, Stoughton WI 53589*
***Consultant*

Abstract. The design of a planar pure permanent magnet undulator is presented. The design requirements and mechanical difficulties for holding, positioning, and driving the magnetic arrays are explored. The structural, thermal, and electrical considerations that influenced the design are then analyzed. And finally detailed magnetic measurements are presented.

Keywords: Insertion Devices, Magnets, Planar Undulator, pure permanent
PACS: 07.07.-a, 07.85.Qe, 07.55.Ge.

INTRODUCTION

Advanced Design Consulting USA, Inc. (ADC) in collaboration with the Synchrotron Radiation Center (SRC), has delivered a new planar pure magnet permanent undulator. This undulator will be the first installed in a short straight section of the Aladdin 1-GeV electron storage ring at SRC. This ID will provide a dedicated, tunable source of approximately 92.5-eV photons for EUV-lithography utilizing the 1st harmonic at both 800-MeV and 1-GeV ring energies. The ID uses a symmetric, planar, pure-permanent magnet design with 41 full-strength poles. End terminations maintain the electron trajectory on-axis – the magnet widths at the exit end are $\lambda/4$, $\lambda/8$, and $1.18\lambda/8$. Functional specifications for the ID are given in Table 1.

MECHANICAL DESCRIPTION

The structure of the planar undulator can be seen in Figure 1. The magnetic gap is controlled by one stepping motor that drives two right/left-hand screwjacks. The single motor drives the lead screws together so that the girders move symmetrically. A phase adjuster is also provided to simplify the removal of taper.

Parameter	Value
Operating temperature Maximum sustainable temperature	25±2°C 35°C
Gap (Pole Face) Orientation	Horizontal, Planar
Magnetic Type	Variable-gap, PPM
Magnetic Period Length, λu	41.6 mm
Mechanical Length Overall	≤ 0.9 m
Number of full-strength, half-period Poles	41
Minimum operational gap, g_{min}	20.5 mm
Minimum on-axis photon energy @ 1 GeV	92.5 eV
Useful harmonics	1st harmonic, only
Phase error	< 7°
Minimum K value (for Operation)	0.5
Maximum gap (for Injection)	80 mm

Table 1: Design objectives for SRC planar PPM ID.

The girders are guided by recirculating roller slides mounted on the strong-back frame, which also supports the jack screw mounts and motor. The frame is mounted to a SRC supplied base with kinematic mounts for adjustment in XYZ directions. The nominal beam height is 1240 mm. Hard stops and optical limits are provided to prevent closing the magnet girders on the beam pipe. A linear encoder tracks the position of the gap. Trim coils correct the slight errors in coupling and electron beam trajectory.

Bi-linear compensation springs are used to eliminate girder float. Their stiffness curves are designed to closely match the magnetic forces.

CONTROL SYSTEM

The control was jointly developed with SRC providing the primary controls and custom inter-

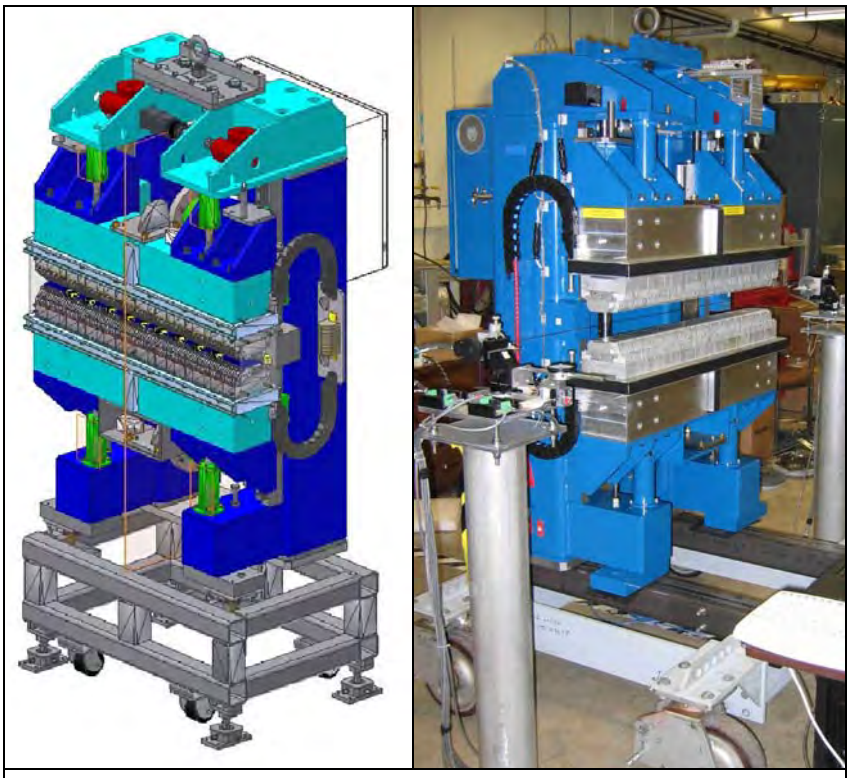

Figure 1: SRC Planar designed by ADC (left) and during flip-coil testing at SRC (right).

face board and ADC providing the power components, limits, encoder and motor controller. The main control resides in a Delta-Tau PMAC PC104 package[1].

A small graphical user interface was written for factory testing and on-site verification using National Instrument's Measurement Studio [2]. The Delta-Tau PMAC controller allows 8 axes of closed loop motion control from a single PC/104 module stack[3]. It can be accessed via the PC/104 bus from a PC/104 CPU or it can operate stand alone via the RS-232 interface. Closed loop operation requires tuning of the PID loop for both servo motor and stepping motor drive systems. The GUI provides a tuning module that drove the gap using a parabolic velocity profile and plotted the following error. The PID parameters are adjusted manually to minimize the following error. Small following errors from mechanical components are compensated in the Delta-Tau firmware by varying the frequency of the stepper motor pulse control. A travel limit interlock composed of five optical limit switches, a key override and a software override was also implemented in the Delta-Tau controller. A time-out feature disables the overrides after 5 minutes if the limit switch trip has not been corrected.

When installed in the storage ring the ID was controlled by a process on the VME computer running under the QNX real-time operating system[4]. The Delta-Tau RS-232 interface was converted to a 10/100 Ethernet interface using a Lantronix XPORT module that was incorporated on the custom control board[5].

TEST RESULTS

A right-hand Cartesian coordinate system is used in all tests with z collinear with the electron path, y vertical-upwards and x horizontal and directed away from the undulator's frame. The measurement laboratory was maintained at a constant temperature of 79 ± 1°F (26 ± 0.6°C) for the duration of the tests.

Girder positioning and deflections

Leveling plates were attached to the undulator at the center of each magnet spar and on the support frame. Roll (theta-z) and pitch (theta-x) measurements were made on the leveling plates in order to verify the mechanical deflections. Results are shown in Figure 2. Changes in roll of <9arcsec and in pitch of <6arcsec attest to the stiffness of the system. The effect of the bilinear springs can be seen in the plot of girder roll, with initial contact at a 35mm gap and a change in stiffness at 25mm.

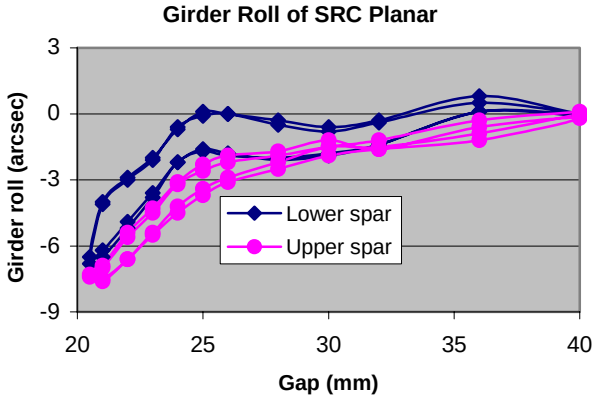

Figure 2: Roll measured on the upper and lower spars.

Multipoles and 2nd integrals

Multipoles were measured at gaps from 20.5 to 80mm using the flip-coil system. Data were taken over a span of ±12mm about the magnetic centerline using 2mm intervals. Five scans were made at each of these positions and the results averaged to reduce the effects of noise. A comparison of results obtained when gaps were reached by opening vs. closing showed no statistical variation. Data at minimum gap are shown in Figure 3.

Second integrals were calculated using the Hall-probe scans and verified using a 180° crossed flip-coil. At large gaps the skew 2nd integral exceeded the specification limit, however, dipole correction was sufficient to bring it into compliance.

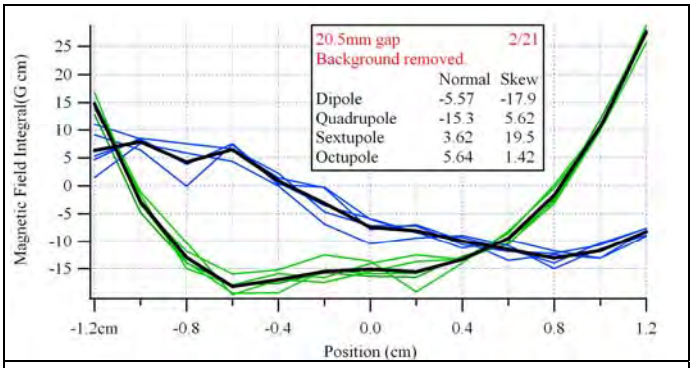

Figure 3: Multipoles measured without correction coils.

Correction coils

Four sets of correction coils have been added to the undulator to correct normal and skew dipoles, skew quadrupole and the normal 2nd integral. The coils were wound within an extruded aluminum carrier mounted directly on the spars. As a result the current in the vertical coil must be changed with the gap.

Mica insulators have been used to provide an air-gap between the coil carriers and the magnet girders in order to reduce heat transfer. Thermocouple measurements on the upper girder showed a temperature rise of about 1°C with a current of 5.5A in the long horizontal coils.

Spectra, orbits and phase errors.

Using ADC's Hall-probe system, the B-fields were scanned along the magnetic axis with samples taken at 1mm intervals. Data was collected along a 2m path starting and ending well beyond the extent of the undulator's magnetic field. Raw data from the Teslameter was thermally compensated in software using linear interpolation of the temperatures taken at the beginning and end of each scan. Misalignments in the individual Hall-sensors were corrected using a 2nd-order compensation scheme. Repeatability was shown to be better than ± 3 G over five scans.

Since drift is a persistent problem with Hall-effect sensors the flip-coil results were used to correct the data. Electron angles calculated from the measured field were corrected to match the integral measured by the flip-coil.

Phase error and trajectories were then calculated from the corrected data. Plots of electron angle, phase error and trajectory are shown in Figure 4 at minimum gap. The transverse field uniformity is also shown in the figure.

The electron angles and pole strengths are plotted in the upper left portion of Figure 4. The blue trace shows the horizontal angle while the vertical angle is shown in green. It is obvious from these plots that the B-fields are featureless at the limits of the scans. Pole strengths are shown as vertical bars and reference the right-hand scale. The spacing between poles 2 and 40 was used to calculate the period, which was found to be 41.623mm. A best fit line through poles 2 - 40 shows a slight taper that can also be seen in the parabolic fit to the phase error plot in the upper right hand portion of the figure. Note that only 41 poles are shown in this plot.

Pole strengths measured at x = ±3mm from the magnetic axis were used to calculate the transverse field uniformity, shown in the lower right portion of the figure. As expected for a PPM device the field variation is very uniform.

Demagnetization

In order to meet the magnetic specifications of this ID it was necessary to use magnets with a high remanence, B_r. Such materials have a relatively low intrinsic coercivity H_{cj}, and special care must be taken to control the demagnetizing field of the undulator.

A detailed model was constructed in Radia [6] to predict the demagnetizing field in a group of five magnets. The center and outer magnets were polarized vertically and the remaining two horizontally. The greatest field was found within the horizontally polarized magnets at a point near the x-y face adjacent to the center pole, just below the x-z face, at x = 0. At this point the demagnetizing field was found to be 19.8 kOe assuming a remanence of 1.32 T.

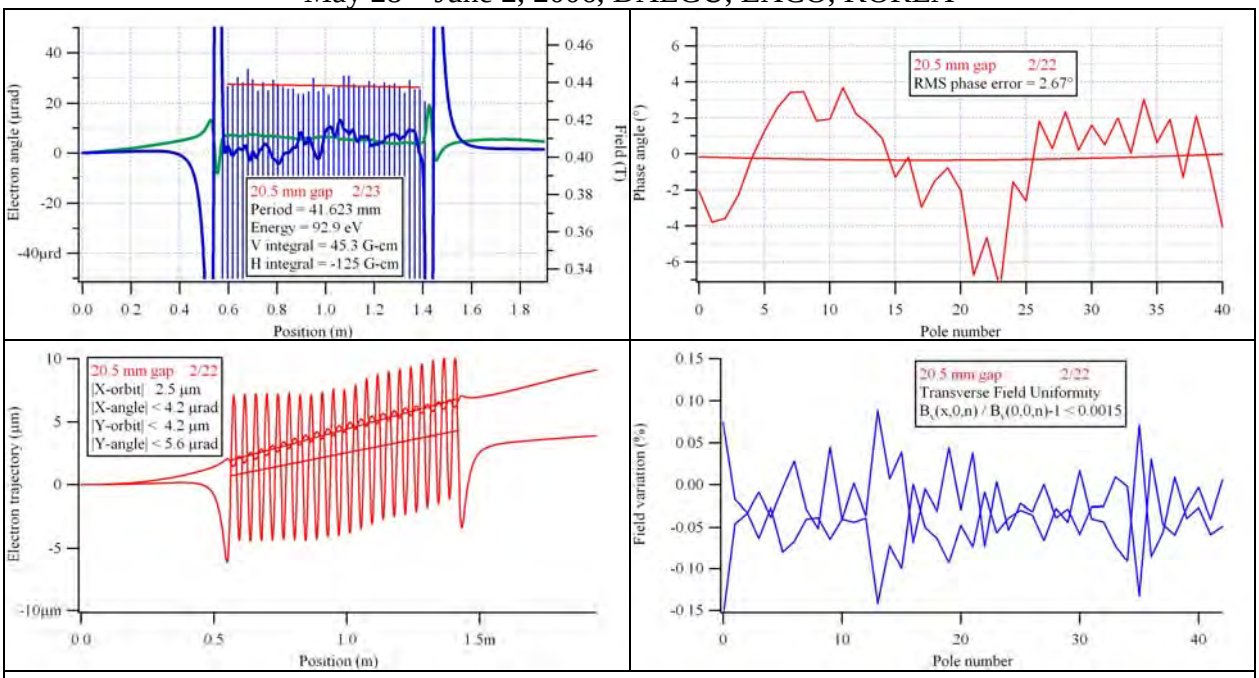

Figure 4: Results for the undulator at minimum gap (20.5 mm). Clockwise from top-left: electron angles and pole strengths; phase error; transverse field uniformity and electron orbits.

The magnets used in the ID have a temperature coefficient for H_{cj} of –0.61 %/°C. If the intrinsic coercivity of the magnets is at the minimum specified value demagnetization could occur at temperatures as low as 29.4°C. If the magnets meet the specified typical value for H_{cj} demagnetization would occur at 42.8°C.

A set of five magnets was assembled and tested to confirm that no damage would occur at the specified environmental temperature limit of 35°C. Measurements were made at room temperature and after sequential eight hour soaks at 30, 35 and 40°C. The By and Bz fields remained stable at temperatures up to at least 35°C. At 40°C degradation was observed. It will be critical to ensure that the undulator is placed at minimum gap if the maximum temperature in the ring exceeds 35°C.

CONCLUSIONS

Commissioning of this device is presently well underway at SRC. Performances, including ring adaptations for vacuum envelope and compensations, are sufficiently encouraging that planning has begun for more aggressive short-straight ID and beamline designs, and attendant scientific program.

ACKNOWLEDGMENTS

This work was supported by the National Science Foundation under Grant No. DMR-0425880 through the Nanoscale Science and Engineering Center and DMR-0084402 through the Synchrotron Radiation Center, both of the University of Wisconsin-Madison.

REFERENCES

[1] http://www.deltatau.com
[2] http://www.ni.com/mstudio/
[3] http://www.pc104.org/
[4] D. E. Eisert, R. A. Bosch, K. D. Jacobs, K. J. Kleman, and J. P. Stott, A New Real-Time Operating System and Python Scripting on Aladdin , PAC 2003 Particle Accelerator Conference May 12-16, 2003.
[5] http://www.lantronix.com
[6] Radia was written at the ESRF by Pascal Elleaume and Oleg Chubar and can be obtained from http://www.esrf.fr